JOURNAL OF SOLID STATE CHEMISTRY **125,** 19–29 (1996)
ARTICLE NO. 0259

Synthesis and Structural Characterization of a New Family of Layered Intergrowth Phases Based on Antimony(III) Oxide

Christopher D. Ling, John G. Thompson, Ray L. Withers, and Siegbert Schmid

Research School of Chemistry, The Australian National University, G.P.O. Box 414, Canberra, ACT, 2601 Australia

Received January 23, 1996; in revised form April 22, 1996; accepted April 25, 1996

A new family of layered oxide phases, described by the general formula $Sb_n^{III}Sb_x^{V}A_{n-x}TiO_{4n+2}$ for $n = 1, 2, 3$ (A = Ta) and $n = 1, 3$ (A = Nb) is reported. Models for the structures of the $n = 1$ and $n = 2$ members are presented, based on the previously reported $n = 3$ structures, XRD, electron diffraction, and microanalytical data. The structures of all members are described as ordered intergrowths of lamellae of the primary oxides of Sb^{III} and Sb^{V}. The other metal atoms are incorporated into lamellae analogous to structures formed by their own primary oxides or binary oxides with Sb^{III}. The structural features of layered antimony oxides as a group, including Sb_2WO_6 and Sb_2MoO_6, are discussed. Antimony oxide-based analogs of the bismuth oxide-based Aurivillius phases appear not to exist in the Sb_2O_3–TiO_2–Nb_2O_5, Sb_2O_3–TiO_2–Ta_2O_5, or related systems.

INTRODUCTION

There are many families of compounds with layered crystal structures consisting of ordered intergrowths of lamellar sheets of simpler structure types. The bismuth oxide-based family of Aurivillius phases (1), many of which are displacive ferroelectrics, is one such example. There are now over 50 known members of this Aurivillius family of phases (2, 3) and the crystal structures of many of these have been determined (4–12). In essence, they consist of a single layer of α-PbO-type ($Bi_2O_2^{2+}$) intergrown with a charge balancing lamellae of perovskite-type ($A_{n-1}B_nO_{3n+1}^{2-}$), n layers thick, to give an overall composition $Bi_2O_2 \cdot A_{n-1}B_nO_{3n+1}$. These two component structure types intermesh by virtue of the commensurability of their ideal basal plane cell dimensions. The large number of different compounds are achieved by the wide variety of combinations of A and B cations which can be accommodated in the n layers thick (n = 1, 2, 3, 4, 5, ...) perovskite lamellae.

By contrast, the $Bi_2O_2^{2+}$ sheet of α-PbO-type has largely been considered to be inviolate. Recent work, however, has demonstrated that other lone-pair-containing cations, such as Pb^{2+}, Sb^{3+}, or Te^{4+}, can be substituted, at least partially, into the $Bi_2O_2^{2+}$ layer (13–16). Castro *et al.* (13), for example, have reported the synthesis of the partly substituted Aurivillius phase $Bi_{2-x}Sb_xSrNb_2O_9$ in the composition range $0 \leq x \leq 1$, but did not observe an Aurivillius phase for $x > 1$. Very recently, however, the $n = 1$ phases Sb_2WO_6 and Sb_2MoO_6 (15–17) have been successfully synthesized. The stoichiometry and obvious layered nature of Sb_2WO_6 and Sb_2MoO_6 suggested the first successful complete substitution of Bi^{3+} (by Sb^{3+}) in the α-PbO layer of any known Aurivillius phase and raised the question of whether or not other fully substituted $n > 1$ Aurivillius phases might exist.

The reported crystal structure of Sb_2WO_6 (15, 17), while showing some similarity to the $n = 1$ Aurivillius phases Bi_2WO_6 and Bi_2MoO_6 (12), nonetheless shows significant differences. First, the single layer perovskite sheet, WO_4^{2-}, is severely distorted from the ideal perovskite type, by an ~25° rotation about a twofold axis of the WO_6 octahedra. This compares with only an ~10° rotation in both Bi_2WO_6 and Bi_2MoO_6 and accounts for the significant difference in a and b basal plane cell dimensions in the case of Sb_2WO_6. Second, the distortion of the $Sb_2O_2^{2+}$ layer from the α-PbO type, particularly the ±~0.6 Å puckering of the square net of oxygens along the stacking direction, is so severe that it is difficult to see how this layer can be considered as being derived from the α-PbO type. This distinction between Bi_2WO_6 and Sb_2WO_6 structure types has recently been demonstrated via a study of the $Bi_{2-x}Sb_xWO_6$ system (16). A clear change in structure type was observed at $x \sim 1.5$.

The implications of these structural differences upon the existence or otherwise of $n > 1$ antimony oxide-based Aurivillius phases led us to this present systematic investigation, in which we have explored the existence of fully substituted $n > 1$ Aurivillius phases in a wide range of systems including Sb_2O_3–SrO–Nb_2O_5, Sb_2O_3–SrO–Ta_2O_5, Sb_2O_3–TiO_2–Nb_2O_5, and Sb_2O_3–TiO_2–Ta_2O_5.

0022-4596/96 $18.00

TABLE 1
Proposed Antimony Oxide-Based Aurivillius Phase Analogs

Aurivillius phase	Proposed phase	Conditions		Major product at equilibrium
		T (°C)	t (h)	
$Bi_2SrTa_2O_9$	$Sb_2SrTa_2O_9$	850	15	no reaction
		1100	15	no reaction
$Bi_2SrNb_2O_9$	$Sb_2SrNb_2O_9$	800	15	no reaction
		1100	15	no reaction
	$Sb_2SrV_2O_9$	700	100	$SrSb_2O_6$
		1100	15	no reaction
$Bi_4Ti_3O_{12}$	$Sb_4Ti_3O_{12}$	850	15	no reaction
		1100	17	no reaction
	$Bi_2Sb_2Ti_3O_{12}$	800	15	$Bi_2Ti_2O_7$
		1100	15	$Bi_2Ti_2O_7$
$Bi_2La_2Ti_3O_{12}$	$Sb_2La_2Ti_3O_{12}$	800	15	$LaTiSbO_6$
		1100	15	$LaTiSbO_6$
	$Sb_2Y_2Ti_3O_{12}$	800	15	$Y_2Ti_2O_7$
		1000	20	$Y_2Ti_2O_7$
Bi_3NbTiO_9	Sb_3NbTiO_9	800	15	$Sb_{1+x}Nb_{1-x}TiO_6$
		1100	15	$Sb_{1+x}Nb_{1-x}TiO_6$
Bi_3VTiO_9	Sb_3VTiO_9	700	100	$SbVO_4$
		1100	15	$SbVO_4$
	$SbVTiO_6$	700	100	$SbVO_4$
		1100	15	$SbVO_4$

SYNTHESIS AND CHARACTERIZATION

Systematic Investigation of Aurivillius Phase Analogs

The range of proposed $n > 1$ antimony oxide-based Aurivillius phase analogs investigated is listed in Table 1. Proposed antimony oxide-based phases without Aurivillius analogs were considered on the basis that smaller A and B cations might be more compatible with the smaller Sb^{3+} cation.

Materials were prepared by solid state reaction between primary oxides at temperatures above the melting point of Sb_2O_3 (656°C). Reactions involving alkaline earths used ternary precursors, $SrTa_2O_6$, $SrNb_2O_6$, or SrV_2O_6, which had been prepared from the alkaline earth carbonates. It was necessary to carry out reactions in sealed platinum tubes, due to the volatility of Sb_2O_3 and the susceptibility of Sb^{3+} to oxidation in air at high temperatures to Sb^{5+}. Reaction times and final annealing temperatures are given in Table 1.

Reaction products were characterized initially by X-ray powder diffraction (XRD) using a Guinier–Hägg camera with Cu$K\alpha_1$ radiation (λ = 1.5406 Å) with Si (NBS No. 640) as an internal standard. Specimens were also examined using a JEOL 6400 scanning electron microscope equipped with a Link ATW detector. Quantitative energy dispersive spectroscopic (EDS) analyses were made at 15 kV and 1 nA with data processed using the Link ISIS system. ZAF corrections were made using the SEMQUANT software package. Ti/Nb ratios were determined using $TiNb_2O_7$ as a standard, precision on the order of 1–2%. Selected specimens were also examined by transmission electron microscopy (TEM) using a Philips EM430 electron microscope (equipped with a PV9900 energy dispersive X-ray detector) and a JEOL 100CX electron microscope.

The results of this systematic investigation are summarized in Table 1, with the majority reaction product identified where reaction occurred.

Investigation of the Sb_2O_3–TiO_2–Nb_2O_5 and Sb_2O_3–TiO_2–Ta_2O_5 Systems

The only new phase discovered during the above systematic investigation had a stoichiometry close to $SbNbTiO_6$, which was clearly inconsistent with the general formula for Aurivillius phases. Compositional analysis of this reaction product in the SEM using EDS gave metal atom ratios ranging from $Sb_{1.0}Nb_{1.0}Ti_{1.0}$ to $Sb_{1.3}Nb_{0.7}Ti_{1.0}$. The variability in Sb and Nb content was ascribed to $Sb^V \leftrightarrow Nb^V$ solid solution, requiring partial oxidation of Sb^{III} to Sb^V. The composition of the proposed solid solution is given as $Sb^{III}Sb^V_xNb^V_{1-x}TiO_6$. Small variations in XRD peak positions in Guinier films from one synthesis to the next supported the hypothesis that this phase occurred over a range of compositions with slightly differing unit cell dimensions.

A single-phase pale yellow powder sample of $Sb_{1+x}Nb_{1-x}TiO_6$, $x \approx 0.0$ was prepared from a stoichiometric mixture of primary oxides heated in a sealed platinum tube to 1150°C for 15 h, cooled to 850°C over 15 h, and then quenched in air. The tantalum-containing analog was prepared in a similar fashion. XRD patterns of these two phases suggested they were isostructural. Attempts to synthesize a vanadium-containing analog were unsuccessful and instead led to formation of $SbVO_4$.

Unit cells for the two new phases were determined from Guinier XRD data using the *ab initio* indexing program VISSER (18) in each case giving monoclinic cells: $Sb_{1+x}Nb_{1-x}TiO_6$, $x \approx 0.0$, a = 5.4971(5), b = 4.8318(5), c = 16.562(2) Å, β = 91.190(1)°; and $Sb_{1+x}Ta_{1-x}TiO_6$, $x \approx 0.0$, a = 5.489(1), b = 4.8171(8), c = 16.670(5) Å, β = 91.144(1)°.

Attempts to grow crystals of $Sb_{1+x}Nb_{1-x}TiO_6$ and $Sb_{1+x}Ta_{1-x}TiO_6$ which were suitable for single crystal X-ray diffraction used the same reaction conditions as for the powder syntheses, except for the addition of a 300% excess of Sb_2O_3 as flux. This led to the growth of transparent yellow, plate-like crystals with dimensions up to 0.10 × 0.10 × 0.02 (niobium-containing synthesis) and 0.05 × 0.05 × 0.01 mm (tantalum-containing synthesis).

XRD showed that the crystals grown by this method were not the desired product. Compositional analysis (EDS) in the SEM found their stoichiometries to be substantially antimony-rich compared with the previously identified phases. Following characterization of these crystals by electron diffraction and structure determination by single crystal X-ray diffraction presented elsewhere (19), they were ascribed the formulas $Sb_3^{III}Sb_x^{V}Nb_{3-x}TiO_{14}$, $0.6 \le x \le 1.3$, and $Sb_3^{III}Sb_x^{V}Ta_{3-x}TiO_{14}$, $0.7 \le x \le 1.8$. The presence of $Sb^{V} \leftrightarrow Nb^{V}$ and $Sb^{V} \leftrightarrow Ta^{V}$ solid solutions was inferred by analogy with the antimony-poor phases. It was not possible to refine the unit cells of these phases from XRD data alone. Reducing the amount of flux failed to produce crystals of the antimony-poor phases; even small excesses of Sb_2O_3 led to the growth of large platey crystals (~1 mm) of the antimony-rich phases among tiny crystallites (5–10 μm) of the antimony-poor phases.

Compositional microanalysis of $Sb_{3+x}Ta_{3-x}TiO_{14}$ crystals sectioned parallel to their platey axis found small intergrown regions with a stoichiometry between those of the so-called antimony-rich and antimony-poor phases. Following electron diffraction analysis, described below, this intermediate phase was ascribed the stoichiometry $Sb_{2+x}Ta_{2-x}TiO_{10}$, $0.7 \le x \le 1.0$. Figure 1 shows a scanning electron micrograph (backscattered electron image) of such a cross section with the intimate intergrowth of the antimony-rich and intermediate composition crystals. Quantitative analyses using EDS from the regions labeled A–E are given in Table 2, together with the derived stoichiometries.

Attempts to synthesize this phase at the derived stoichiometry in the Sb_2O_3–TiO_2–Ta_2O_5 system were unsuccessful, the phase only ever being observed as an intergrowth with $Sb_{3+x}Ta_{3-x}TiO_{14}$. Surprisingly, it was not possible to prepare the niobium analog, $Sb_{2+x}Nb_{2-x}TiO_{10}$. It was never observed by electron diffraction in specimens of $Sb_{3+x}Nb_{3-x}TiO_{14}$.

In the following sections we describe the five newly observed phases by the general formula $Sb_n^{III}Sb_x^{V}A_{n-x}TiO_{4n+2}$ for $n = 1, 2, 3$ (A = Ta) and $n = 1, 3$ (A = Nb).

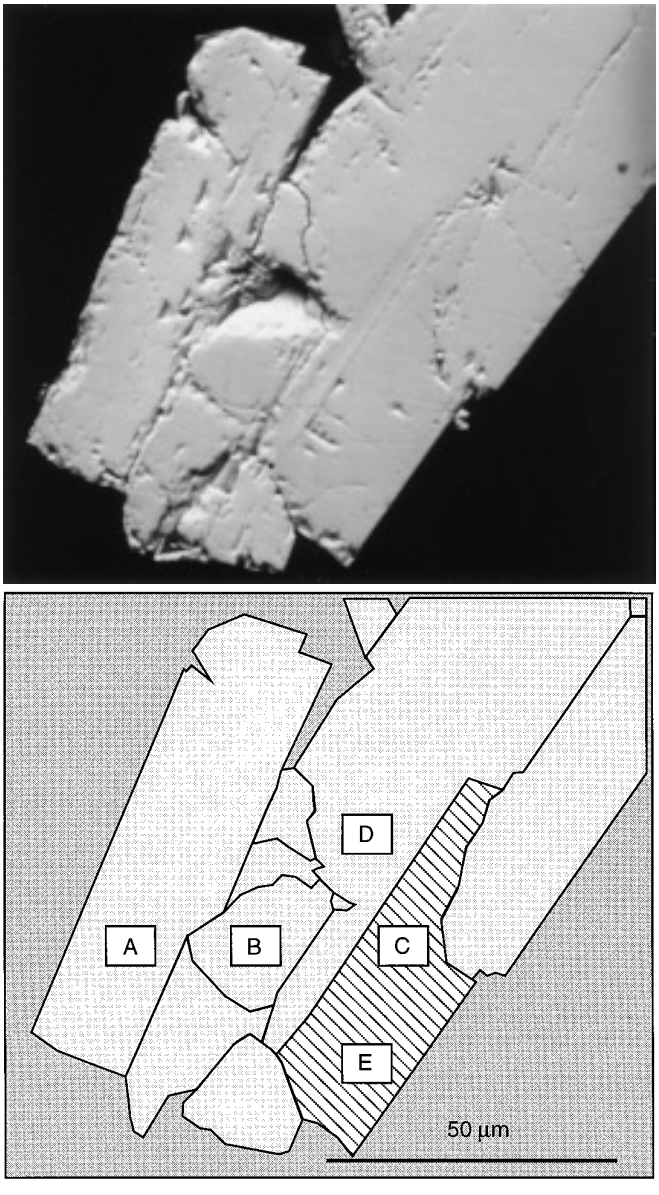

FIG. 1. Scanning electron micrograph (backscattered electron image) of a cluster of $Sb_3^{III}Sb_x^{V}Ta_{3-x}TiO_{14}$ crystals sectioned parallel to their platey axes with an intimate intergrowth (striped region) of $Sb_2^{III}Sb_x^{V}Ta_{2-x}TiO_{10}$. The labeled rectangular regions correspond to the EDS microanalyses given in Table 2.

ELECTRON DIFFRACTION STUDY OF $Sb_n^{III}Sb_x^{V}(Nb, Ta)_{n-x}TiO_{4n+2}$

n = 1 Phase

Single phase powders of $Sb_1^{III}Sb_x^{V}Nb_{1-x}TiO_6$ and $Sb_1^{III}Sb_x^{V}Ta_{1-x}TiO_6$ were studied by electron diffraction. Microdiffraction patterns (DPs) taken down the (a) [100], (b) [010], and (c) [001] zone axes of $Sb_{1+x}Nb_{1-x}TiO_6$ are shown in Fig. 2. Note the systematic absences hkl, $k + l = 2n + 1$ and $h0l, h, l = 2n + 1$; these extinction conditions are compatible with space group symmetries $A1a1$ and $A12/a1$. These nonstandard settings were retained in light of the likelihood that this was a layered structure similar to Aurivillius phases; the long axis is always the stacking axis in Aurivillius phases, and is conventionally labeled **c**. DPs for $Sb_1^{III}Sb_x^{V}Ta_{1-x}TiO_6$ were found to be entirely analogous.

n = 3 Phase

A TEM and single crystal X-ray diffraction study of $Sb_3^{III}Sb_x^{V}Nb_{3-x}TiO_{14}$ and $Sb_3^{III}Sb_x^{V}Ta_{3-x}TiO_{14}$ (19) identified

TABLE 2
Compositional Analyses of Regions Shown in Fig. 2.

Analysis	Wt% Sb_2O_4	Wt% Ta_2O_5	Wt% TiO_2	(Sb + Ta) : Ti	x^a
A	53.8	39.5	6.7	6.34	1.00
B	67.9	24.8	7.4	6.00	1.79
C	55.2	35.5	9.3	4.47	0.82
D	59.5	33.5	7.0	6.17	1.33
E	59.5	30.7	9.8	4.29	0.98

[a] Assumes partial substitution of Ta for Ti on Ti site. Analyses A, B, and D use the formula $Sb_3^{III}Sb_x^{V}Ta_{3-x}TiO_{14}$ while analyses C and E use the formula $Sb_2^{III}Sb_x^{V}Ta_{2-x}TiO_{10}$.

basal plane unit cell dimensions similar to those of $Sb_1^{III}Sb_x^{V}Nb_{1-x}TiO_6$ and $Sb_1^{III}Sb_x^{V}Ta_{1-x}TiO_6$, but with a much longer **c** axis. The unit cells, refined by least-squares from Guinier XRD data, were $Sb_3^{III}Sb_x^{V}Nb_{3-x}TiO_{14}$, a = 4.8685(1), b = 5.5241(1), c = 40.217(1) Å, β = 91.00(2)° and $Sb_3^{III}Sb_x^{V}Ta_{3-x}TiO_{14}$, a = 4.818(3), b = 5.511(4), c = 40.12(3) Å, β = 91.08(2)°. The extinction conditions observed for these two phases (19) were again consistent with the space groups $A1a1$ or $A12/a1$.

It was noted that every seventh reflection along the **c*** direction (i.e., the allowed reflections $(0, 0, 14n)$, where n is an integer) dominated the pattern of reflection intensities. This indicated a structural repeat along z of $c/14$, i.e., 2.87 Å, such as the average metal atom spacing in a layered oxide structure.

n = 2 Phase

Ground crystals of $Sb_3^{III}Sb_x^{V}Ta_{3-x}TiO_{14}$ found by EDS to contain intergrowths of $Sb_2^{III}Sb_x^{V}Ta_{2-x}TiO_{10}$ were studied by electron diffraction. DPs taken down the (a) [100], (b) [010], and (*c*) [001] zone axes of $Sb_2^{III}Sb_x^{V}Ta_{2-x}TiO_{10}$ are shown in Fig. 3. Note the systematic absences $h0l$, $h = 2n + 1$, $0kl$, $l = 2n + 1$ and $hk0$, $h + k = 2n + 1$; these extinction conditions uniquely determine space group symmetry *Pcan*. The orthorhombic unit cell was determined within the accuracy of electron diffraction; $a \approx 5.5$, $b \approx 4.8$, $c \approx 28.7$ Å. In the absence of a single phase powder for XRD, this cell could not be refined further.

The spacing corresponding to the dominant reflections in the n = 2 DPs (2.87 Å) is identical to the spacing corresponding to the dominant reflections for the n = 3 phases. This observation, combined with the similar basal plane (a and b) dimensions for the n = 1, 2 and 3 unit cells, implies that all are built out of similar intergrown units. This would give different c dimensions, but the same average metal atom spacing, as observed. Structural models based on this hypothesis are presented below for the n = 1 and 2 phases along with supporting evidence.

MODELS FOR THE n = 1 AND n = 2 STRUCTURES

Description of the n = 3 Structure

The structures of the n = 3 phases, $Sb_3^{III}Sb_x^{V}Nb_{3-x}TiO_{14}$ and $Sb_3^{III}Sb_x^{V}Ta_{3-x}TiO_{14}$, have been solved and refined (19), and shown to be isomorphous, layered intergrowth structures. The structure for n = 3 has been described as an ordered intergrowth of lamellae of β-Sb_2O_4 (20) and Sb_2O_5 (21) structure types, with "twin planes" perpendicular to [001] similar to those observed in α-Sb_2O_4 (22).

To understand this description of the structures of the n = 3 phases, and the models proposed later for the n = 1 and 2 phases, it is helpful to refer to the work of Hyde and Andersson (23) (see also (24)). They provide an elegant structural relationship between the various oxides of antimony by focusing on the oxygen plus lone pair (E) array. Figure 4a shows the real structure of α-Sb_2O_3 (25) in which the Sb^{3+} ions occupy approximate tetrahedral coordination, SbO_3E. When idealized, as in Fig. 4b, it is now evident that the oxygens and lone pairs form a twinned hcp array, with Sb^{3+} ions occupying approximate trigonal bipyramidal coordination, SbO_4E. The $\{\bar{1}101\}_{hcp}$ twin planes joining the twin blocks are marked by arrows in Fig. 4b. The beauty of this description is that the relationship of α-Sb_2O_3 to α-Sb_2O_4 (Fig. 4c) is immediately apparent. In α-Sb_2O_4, every second Sb is pentavalent and occupies an SbO_6 octahedron. Half of the lone pairs have been replaced by oxygens, and the oxidized antimony ions have moved from trigonal bipyramidal to octahedral coordination, but the twinned hcp array remains invariant. The relationship between the structures of β-Sb_2O_4 and Sb_2O_5 (Figs. 4d and 4e, respectively) can be similarly understood. The only difference in this case is that the invariant hcp array is untwinned.

The crystal structure of the idealized n = 3 structure presented in terms of its β-Sb_2O_4-type and Sb_2O_5-type building blocks is shown in Fig. 5a. The octahedra in the actual n = 3 structures are rotated slightly around **a** and **c** relative to this idealized representation (19). Two mixed atom sites were determined from the refinement and are indicated in Fig. 5a. When considering substitution onto these sites, it is significant that the same substitutions with preservation of structure type are observed in simple oxide structures (23). Thus $SbNbO_4$ is isostructural with α-Sb_2O_4 and B-Nb_2O_5 with Sb_2O_5. Similarly, rutile (TiO_2) consists of extended edge-shared layers of corner-shared octahedra such as the two consecutive edge-shared layers found in Sb_2O_5.

Proposed n = 1 and n = 2 Structural Models

Given that the n = 1, 2 and 3 phases comprise a homologous compositional series and share nearly identical basal plane dimensions, it is reasonable to attempt to construct

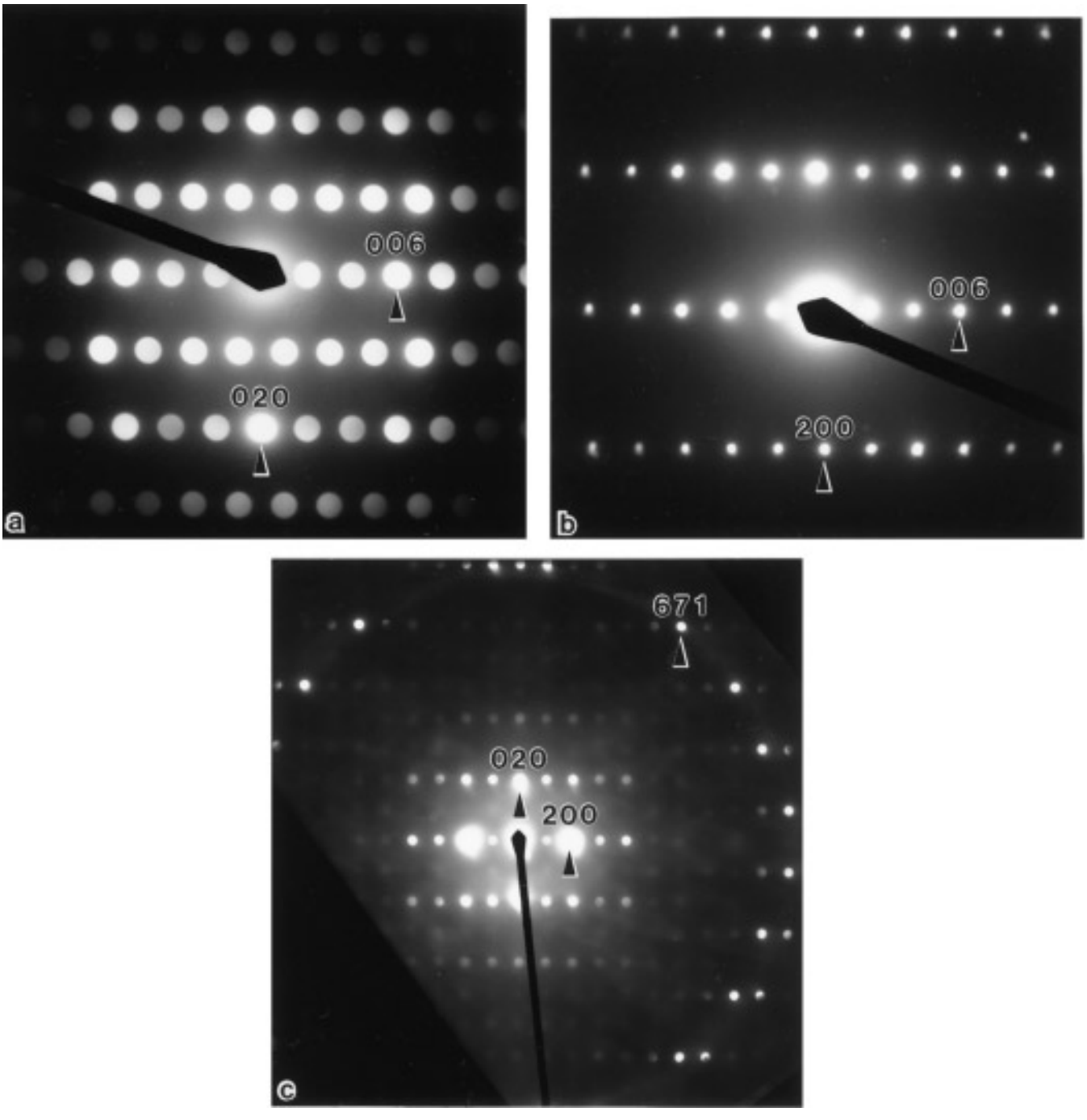

FIG. 2. Electron microdiffraction patterns of $Sb_1^{III}Sb_x^{V}Nb_{1-x}TiO_6$ along the (a) [100], (b) [010], and (c) [001] zone axes.

models of the lower order phases from the building blocks of the $n = 3$ phase. In constructing these models it is assumed that mixed occupancy of metal sites observed in the $n = 3$ phases also applies to the equivalent building blocks in the $n = 1$ and 2 phases. Unit cell and space group symmetry information for this series and various other antimony oxides is summarized in Table 3.

The c dimensions of the $n = 1$ and 2 phases are successively approximately 12 Å shorter than the $n = 3$ phase. Considering the average layer spacing in the $n = 3$ phase, 40.2/14 = 2.87 Å, this suggests that the $n = 2$ phase is made up of 10 such layers and the $n = 1$ phase of 6 such layers. These conclusions are supported by electron diffraction evidence; the average

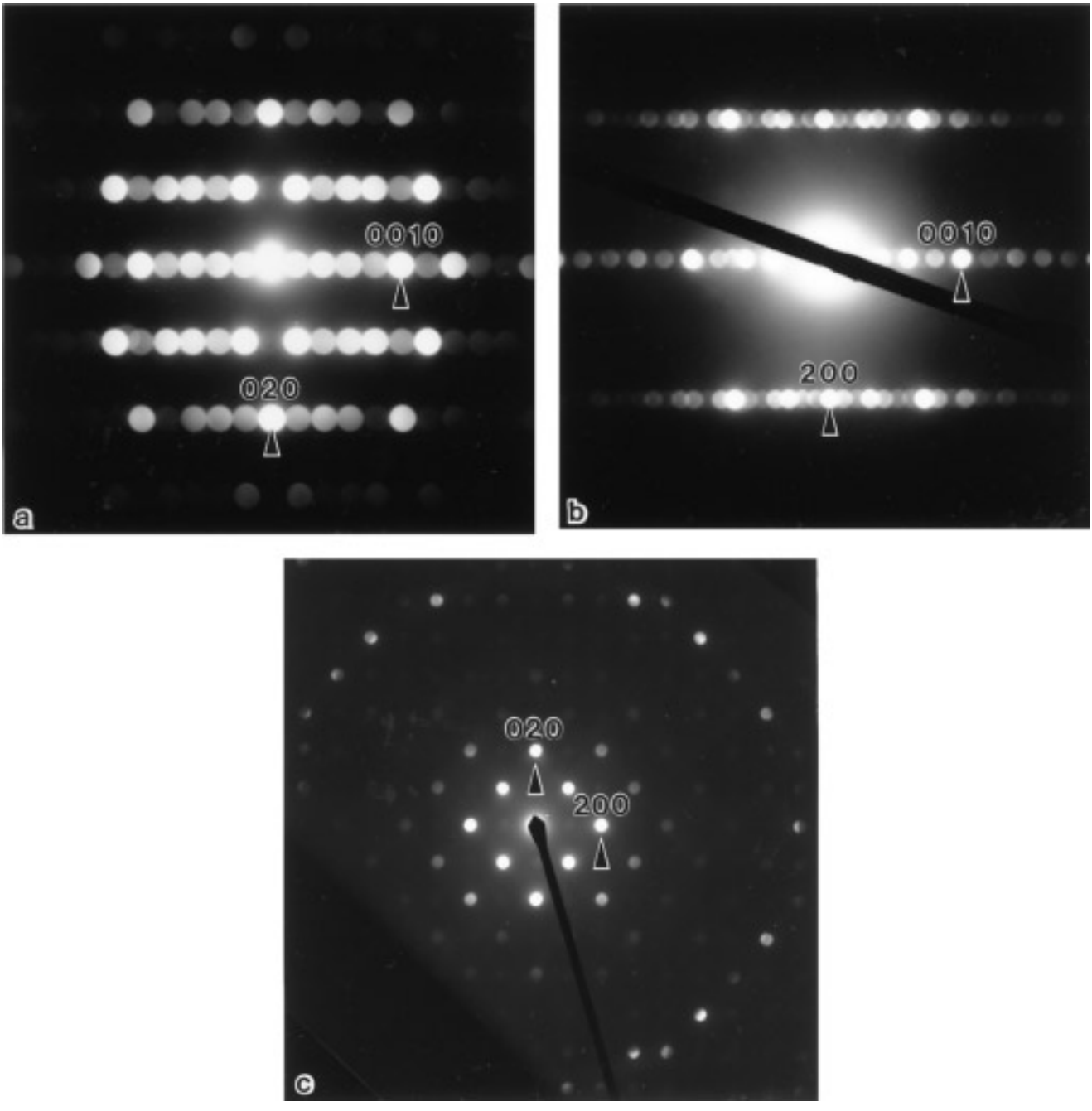

FIG. 3. Electron microdiffraction patterns of $Sb_2^{III}Sb_x^{V}Ta_{2-x}TiO_{10}$ along the (a) [100], (b) [010], and (c) [001] zone axes.

layer spacing in the $n = 3$ phase is indicated by a strong (0, 0, 14) reflection at 0.35 $Å^{-1}$, the same reciprocal lattice spacing corresponding to (0, 0, 10) in the $n = 2$ phase and (006) in the $n = 1$ phase.

The presence of titanium in the $n = 2$ phase indicates that it must contain rutile-type units. Considering this, and the symmetry elements required, the only possible arrangement of 10 layers from the $n = 3$ structure is that shown in Fig. 5b. The same combination of composition and symmetry arguments leads to an unambiguous model for the $n = 1$ phase, shown in Fig. 5c. Atomic coordinates for this latter model derived from the $n = 3$ structure (19) are listed in Table 4. This model was tested (see below) by comparison of the observed and calculated XRD profiles using the Rietveld method. A full unconstrained refinement of the structure was not possible due to the dominant contribution of the metal atoms to the structure factors, which precluded refinement of the oxygen atom positions.

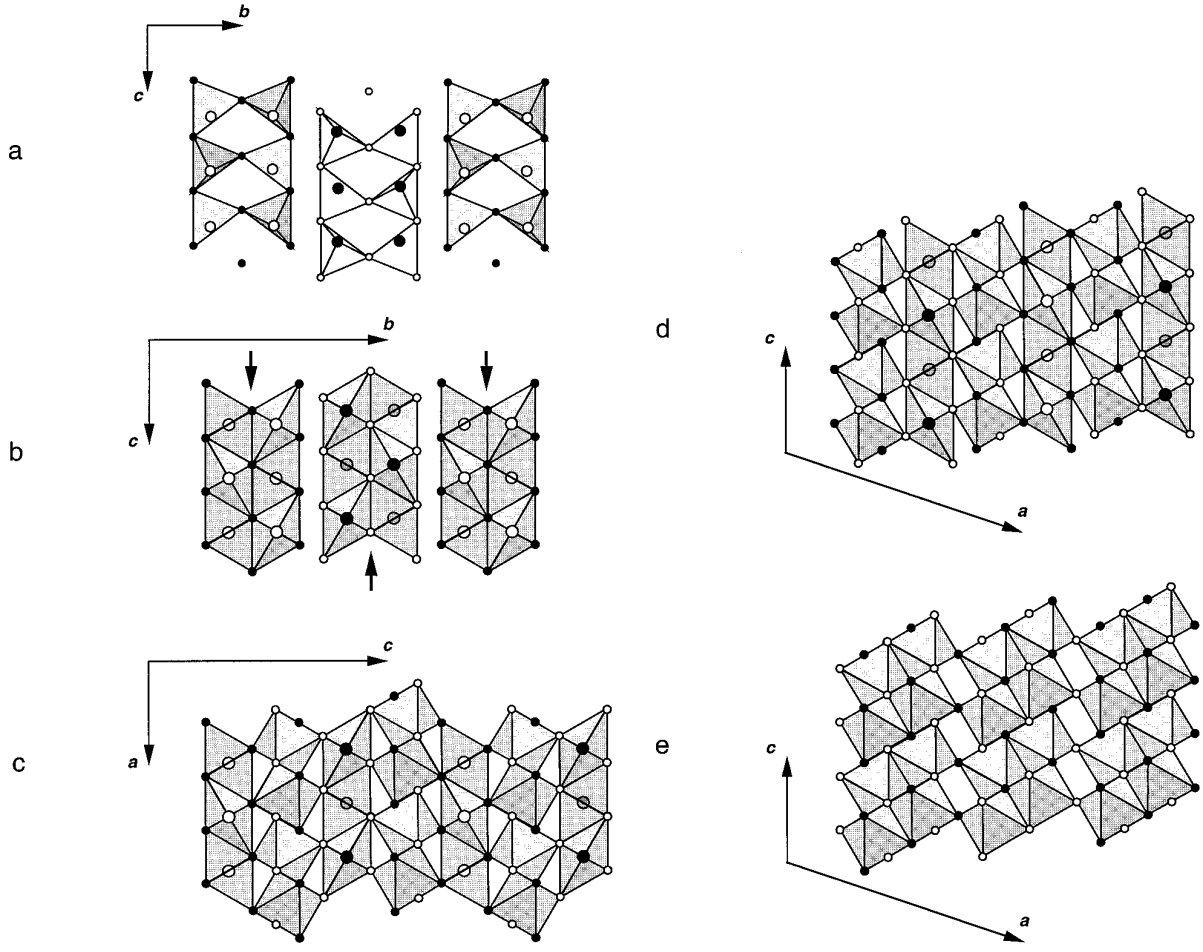

FIG. 4. Schematic polyhedral representations of the real structure of α-Sb_2O_3 (a) and idealized representations of α-Sb_2O_3 (b), α-Sb_2O_4 (c), β-Sb_2O_4 (d), and Sb_2O_5 (e). Oxygens are represented by small circles and lone pairs by large circles, the black circles being at a height of 0 and white circles at a height of 1/2. The hcp arrays of oxygens plus lone pairs can be seen in the alternating black and white vertical rows.

Testing the n = 1 Structural Model

XRD data used were of an approximately single phase powder specimen of $Sb^{III}_1Sb^{V}_xNb_{1-x}TiO_6$ ($x \approx 0.26$). Numerical intensities were obtained by measuring the Guinier–Hägg film with a densitometer with nominal resolution of $0.02°\theta$. Data were corrected for the geometric factor associated with use of a Guinier–Hägg camera ($G = 1/\cos(2\theta - \phi)$, where $\phi = 30°$) (26).

Refinement was performed using the program DBW3.2 (27) with all data from 18 to 78° 2θ. Refinement of scale, zero correction, peak profile parameters, unit cell dimensions, and thermal parameters gave an R_{Bragg} of 6.5% ($R_{Bragg} = 100\ \Sigma\ |I_{obs} - I_{calc}|/\Sigma I$). Refinement of the metal atom positions improved the refinement only slightly. Figure 6 shows the observed, calculated, and difference XRD profiles for this model. Most of the misfit between observed and calculated data is due to imperfect modeling of the peak profile, though there are some significant under- and overcalculations observable. Calculation of bond valence sums (28) for the $n = 3$ derived model (see Table 4) shows that it is chemically quite plausible.

DISCUSSION

$Sb^{III}_nSb^{V}_x(Nb, Ta)_{n-x}TiO_{4n+2}$ vs $Bi_2O_2 \cdot A_{n-1}B_nO_{3n+1}$

The phases represented in Fig. 5 comprise a homologous series of layered intergrowth structures. The only sense in which this is not the case is in the location of ordered twin planes, the most subtle feature of the structures. In this sense, they may be thought of as an antimony oxide-based counterpart to the bismuth oxide-based Aurivillius series of layered intergrowth phases. However, the analogy soon breaks down as the units containing the key cations are quite different. Bi^{3+} is incorporated into the $Bi_2O_2^{2+}$ layers of Aurivillius phases in α-PbO-type units, whereas in the layered antimony oxide-based phases presented in this pa-

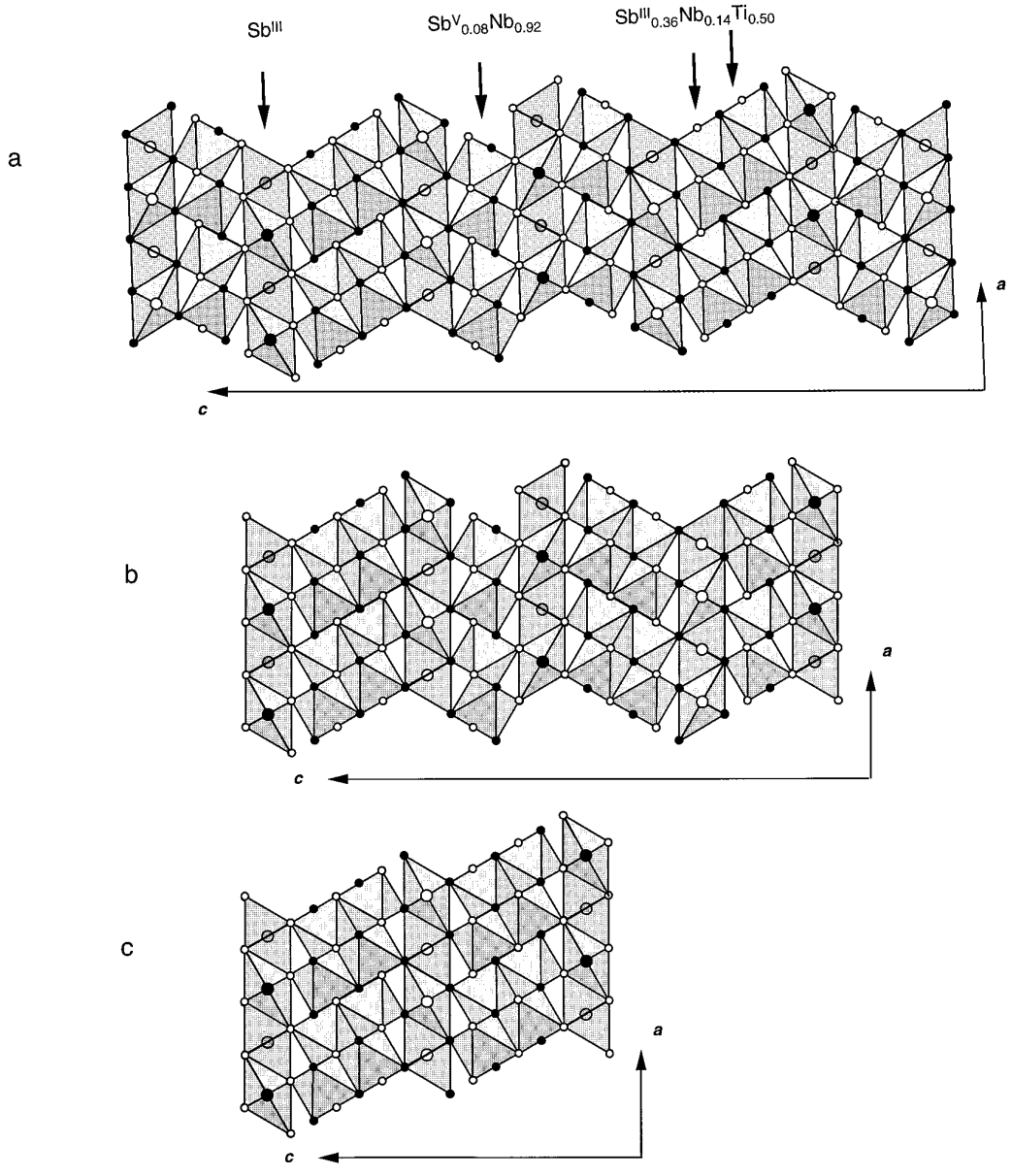

FIG. 5. Schematic polyhedral representations of $Sb^{III}_nSb^{V}_xA_{n-x}TiO_{4n+2}$ for (a) $n = 3$, (b) $n = 2$, and (c) $n = 1$ projected along the [010] direction. As in Fig. 4, the hcp arrays of oxygens plus lone pairs can be seen in the alternating black and white vertical rows.

per, Sb^{3+} is present in quite distinct, single layer, α-Sb_2O_3 units (compare Fig. 4b with Fig. 5). It is the apparent rigidity of this single layer, α-Sb_2O_3 unit which enforces a hcp (or twinned hcp) oxygen (plus lone pair) array and requires that any intergrown octahedral layer is based on an hcp oxygen array. Such an hcp array of oxygen atoms and electron lone pairs is incompatible with the ReO_3-type oxygen array of the block structures characteristic of the TiO_2–Nb_2O_5 and TiO_2–Ta_2O_5 binary systems (29, 30).

Table 3 lists unit cell dimensions and space group symmetries of representatives of each structure type observed as components in the layered antimony oxides, juxtaposed to the unit cell dimensions of the $n = 1$ and 3 phases. Where necessary, axis labels have been permuted for ease of comparison. The relative invariance of the basal plane dimensions normal to the stacking direction, 5.5×4.8 Å, is in keeping with the dimensions of the hcp oxygen (plus lone pair) array. It is ultimately this common basal plane which makes intergrowth of the structural components of the new layered antimony oxide-based phases possible.

The oxygen plus lone pair (E) hcp based description of layered antimony oxide-based phases places the descrip-

TABLE 3

Comparison of Unit Cells and Space Group Symmetries for Various Antimony Oxides and Layered Antimony Oxide-Based Structures

Compound	a (Å)	b (Å)	c (Å)	β (°)	Space group	
α-Sb_2O_3	5.42	4.92	12.46	—	*Pnaa*	(25)
α-Sb_2O_4	5.46	4.81	11.78	—	$Pna2_1$	(22)
β-Sb_2O_4	5.38	4.83	12.06	104.6	*A*12/*a*1	(20)
Sb_2O_5	5.42	4.78	12.65	103.9	*A*12/*a*1	(21)
Sb_2WO_6[a]	11.12	9.90	18.48	96.9	$F\bar{1}$	(17)
$Sb_{3+x}Nb_{3-x}TiO_{14}$	5.52	4.87	40.12	91.00	*A*12/*a*1	(19)
$Sb_{2+x}Ta_{2-x}TiO_{10}$	5.5	4.8	28.7	—	*Pcan*	—
$Sb_{1+x}Nb_{1-x}TiO_6$	5.50	4.83	16.56	91.19	*A*12/*a*1	—

[a] Sb_2WO_6 is metrically triclinic; $\alpha = 90.2°$, $\gamma = 90.2°$.

tion of Sb_2WO_6 and Sb_2MoO_6 as direct antimony oxide-based analogs of $n = 1$ Aurivillius phases in some doubt (15). These phases are rather better represented as ordered intergrowths of lamellae of β-Sb_2O_4 and α-Sb_2O_3-type (compare Fig. 7a with Fig. 4b and 4d). The hcp (oxygen plus lone pair) description implies that Sb^{3+} is much better described as being incorporated into Sb_2WO_6 in the form of double layer, α-Sb_2O_3-type units rather than as being incorporated in the form of α-PbO-type units (compare Fig. 4b with Fig. 7a). Similarly, the hcp (oxygen plus lone pair) description requires that the single octahedral layers present in Fig. 7a (and Fig. 5) are much more appropriately described as single $(1\ \bar{1}01)$ layers of PdF_3 type (see Chap. 4 of (22)) rather than as single layers of perovskite type.

Furthermore, the hcp description suggests the nature of the problem in forming direct antimony oxide-based Aurivillius analogs where $n > 1$. An idealized structural model for such a hypothetical $n = 2$ phase is represented in Fig. 7b. In this model, the ''perovskite'' octahedra have been rotated by 30° about a cubic perovskite [111] axis to the PdF_3-type configuration (23), whereby the initially 12 coordinate perovskite *A*-type site is transformed into a trigonal site far too small to accommodate the *A*-site cations typical of known Aurivillius phases. This helps explain the nonobservance of $n > 1$ antimony oxide-based Aurivillius analogs in this and previous studies (14). In PdF_3-type octahedral arrays, the perovskite *A* site effectively no longer exists. There are, however, neighboring relatively small octahedral interstices adjacent to the trigonal site mentioned above which can be occupied but only if the interstitial cation is sufficiently small, e.g., Li^+ in the $LiNbO_3$ (23) structure. The need for the intergrown structural component to be compatible with single layer units of the α-Sb_2O_3 type appears to explain the absence of perovskite-type lamellae in these antimony oxide-based phases.

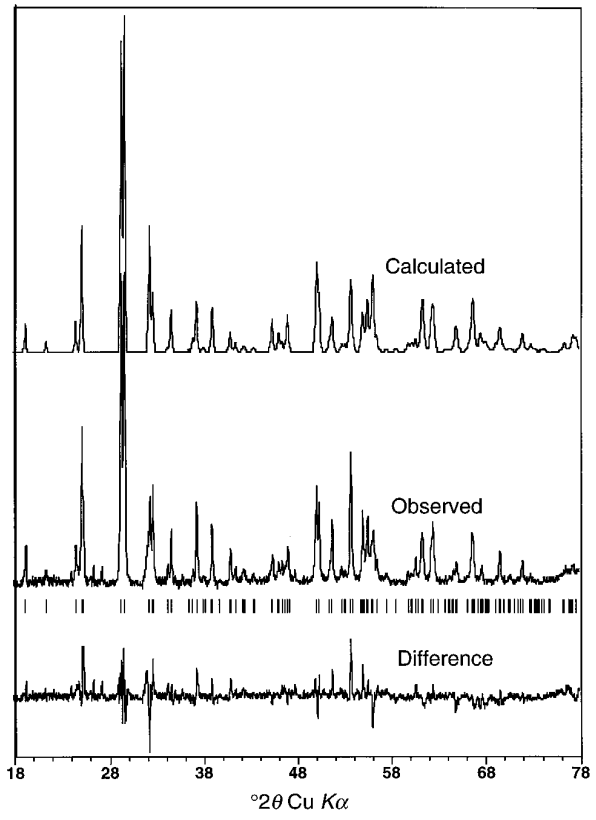

FIG. 6. Observed, calculated, and difference XRD profiles of the $n = 3$ derived model for $Sb_1^{III}Sb_x^{V}Nb_{1-x}TiO_6$ ($x = 0.26$).

TABLE 4

Atomic Coordinates and Bond Valence Sums for the $Sb_1^{III}Sb_{0.26}^{V}Nb_{0.74}TiO_6$ Structure Model Derived from the $n = 3$ Structure

Atom	x	y	z	Bond[a] valence sum	Expected valence
Sb^{III}	0.0	0.704	0.25	2.7	3.0
$Sb_{0.13}Nb_{0.37}Ti_{0.5}$	0.172	0.242	0.167	4.6	4.5
O1	0.072	0.414	0.101	2.2	2.0
O2	0.222	0.565	0.362	1.9	2.0
O3	0.141	0.048	0.444	1.9	2.0

[a] R_0Sb^{III}–O = 1.973, $R_0(Sb_{0.13}Nb_{0.37}Ti_{0.5})$–O = 1.867 derived from reference 28. S.G. *C*2/*c*:, $Z = 4$; $a = 16.668(2)$, $b = 4.830(1)$, $c = 5.499(1)$ Å, $\beta = 91.07(1)°$.

Extending the Layered Antimony Oxide-Based Phases

Much potential exists for future work on the layered antimony oxide-based phases described in this paper. Further work is required, for example, on the $Sb_n^{III}Sb_x^{V}$

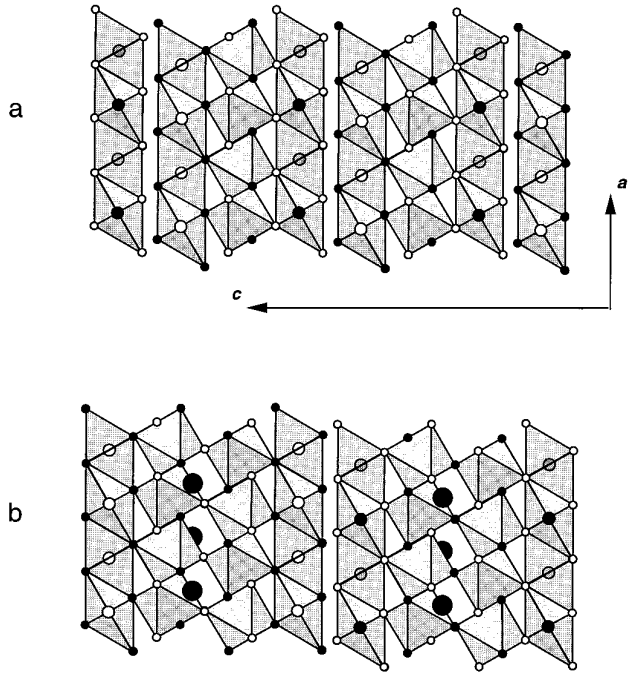

FIG. 7. Idealized schematic polyhedral representation of Sb_2WO_6 as an ordered intergrowth of α-Sb_2O_3-type and β-Sb_2O_4-type structures (a), and a hypothetical structure in which the single PdF_3-type layer has been replaced by two layers of $LiNbO_3$-type structure (b).

$A_{n-x}TiO_{4n+2}$ family itself to establish the range of solid solution for each value of n. Synthesis of the phases under reducing conditions would presumably give the end members where $x = 0$. The $n = 2$ member from the Sb_2O_3–TiO_2–Nb_2O_5 system might be obtained in this way. Being able to restrict compositional variation, i.e., the range of x, should lead to growth of better crystals and hence better structure refinements.

Beyond further investigation of the $Sb_{n+x}A_{n-x}TiO_{4n+2}$ family itself, it remains to try and extend it, through inclusion of different structure types and/or cation arrangements in the non-α-Sb_2O_3-type lamellae. Given the discussion in the previous section, it would first be of interest to reinvestigate direct antimony oxide-based Aurivillius analogs, by attempting to intergrow the α-Sb_2O_3-type units observed in Sb_2WO_6 and Sb_2MoO_6 with extended slabs of n layers thick $LiNbO_3$-type structure ($Li_{n-1}B_nO_{3n+1}^{2-}$) to give an overall composition $Sb_2O_2 \cdot Li_{n-1}B_nO_{3n+1}$ directly analogous to the Aurivillius phases.

Clearly any pseudo-hcp material with compatible basal plane dimensions could potentially intergrow with single layer units of the α-Sb_2O_3-type. Possibilities that immediately spring to mind include yellow PbO and α-PbO_2 (23). The rutile-related phase $SbVO_4$ (31) might also be compatible. Inclusion of lamellae of new structure types or of the same structure type but with different composition will require careful consideration of factors such as overall charge balance, cation size, and other crystal chemical considerations.

CONCLUSION

Antimony oxide-based analogs of the bismuth oxide-based Aurivillius phases appear not to exist in the Sb_2O_3–TiO_2–Nb_2O_5, Sb_2O_3–TiO_2–Ta_2O_5, or related systems. This results from the incompatibility of the α-Sb_2O_3-type unit with the perovskite-type units associated with Aurivillius phases. The α-Sb_2O_3-type unit is, however, compatible with the β-Sb_2O_4 and Sb_2O_5 structure types, and this leads to the formation of a new family $Sb_n^{III}Sb_x^{V}A_{n-x}TiO_{4n+2}$ of layered intergrowth compounds. The fundamental building blocks of this new family of compounds are a single layer unit of α-Sb_2O_3-type and a single $(1\bar{1}01)$ layer unit of PdF_3-type. The differing ways in which these building blocks might be stacked suggests great potential flexibility. The clear structural differences between this new family of phases and Aurivillius phases suggests they will not have the same physical properties. The new family of phases, for example, are centrosymmetric, ruling out the displacive modes responsible for ferroelectricity in the latter (12). A more systematic investigation of these systems is planned.

REFERENCES

1. B. Aurivillius, *Ark. Kemi* **1,** 463 (1949).
2. E. C. Subbarao, *Ferroelectrics* **5,** 267 (1973).
3. K. Singh, D. K. Bopardikare, and D. V. Atkare, *Ferroelectrics* **82,** 55 (1988).
4. R. W. Wolfe, R. E. Newnham, D. K. Smith, and M. I. Kay, *Ferroelectrics* **3,** 1 (1971).
5. J. F. Dorrian, R. E. Newnham, D. K. Smith, and M. I. Kay, *Ferroelectrics* **3,** 17 (1971).
6. F. Theobald, A. Laarif, and A. W. Hewat, *Ferroelectrics* **56,** 219 (1984).
7. A. D. Rae, J. G. Thompson, R. L. Withers, and A. C. Willis, *Acta Crystallogr. Sect. B* **46,** 474 (1990).
8. A. D. Rae, J. G. Thompson, and R. L. Withers, *Acta Crystallogr. Sect. B* **47,** 870 (1991).
9. J. G. Thompson, A. D. Rae, R. L. Withers, and D. C. Craig, *Acta Crystallogr. Sect. B* **47,** 174 (1991).
10. A. D. Rae, J. G. Thompson, and R. L. Withers, *Acta Crystallogr. Sect. B* **48,** 418 (1992).
11. J. G. Thompson, S. Schmid, R. L. Withers, A. D. Rae, and J. D. Fitz Gerald, *J.Solid State Chem.* **101,** 309 (1992).
12. R. L. Withers, J. G. Thompson, and A. D. Rae, *J.Solid State Chem.* **94,** 404 (1991).
13. A. Castro, P. Millán, M. J. Martinez-Lope, and J. B. Torrance, *Solid State Ionics* **63–65,** 897 (1993).
14. P. Millan, A. Castro, and J. B. Torrance, *Mater. Res. Bull.* **28,** 117 (1993).
15. A. Castro, P. Millán, R. Enjalbert, E. Snoeck, and J. Galy, *Mater. Res. Bull.* **29,** 871 (1994).
16. A. Castro, P. Millan, and R. Enjalbert, *Mater. Res. Bull.* **30,** 871 (1995).
17. C. D. Ling, R. L. Withers, A. D. Rae, S. Schmid, and J. G. Thompson, *Acta Crystallogr. Sect. B*, in press.
18. J. W. Visser, *J. Appl. Crystallogr.* **2,** 89 (1969).
19. C. D. Ling, S. Schmid, J. G. Thompson, and R. L. Withers, submitted for publication.

20. D. Rogers and A. C. Skapski, *Proc. Chem. Soc.* 400 (1964).
21. M. Jansen, *Acta Crystallogr. Sect. B* **35,** 539 (1979).
22. P. S. Gopala Krishnan and H. Manohar, *Cryst. Struct. Commun.* **4,** 203 (1975).
23. B. G. Hyde and S. Andersson "Inorganic Crystal Structures." Wiley, New York, 1989.
24. S. Andersson and A. Åström, *Nat. Bur. Stand. Special Publ.* **364,** 3 (1972).
25. C. Svensson, *Acta Crystallogr. Sect. B* **30,** 458 (1974).
26. G. Malmros and P.-E. Werner, *Acta Chem. Scand.* **27,** 493 (1973).
27. D. B. Wiles and R. A. Young, *J. Appl. Crystallogr.* **14,** 149 (1981).
28. N. E. Brese and M. O'Keeffe, *Acta Crystallogr. Sect. B* **47,** 192 (1991).
29. R. S. Roth, J. R. Dennis, and H. F. McMurdie (Eds.), "Phase Diagrams for Ceramists," Vol. VI, Figs. 6522 and 6523. American Ceramic Society, 1987.
30. E. M. Levin and H. F. McMurdie (Eds.), "Phase Diagrams for Ceramists," Vol. IV, Fig. 4454. American Ceramic Society, 1975.
31. A. Landa-Cànovas, J. Nilsson, S. Hansen, K. Stahl, and A. Andersson *J. Solid State Chem.* **116,** 369 (1995).